ELSEVIER

International Journal of Mass Spectrometry 208 (2001) 17–27

International Journal of Mass Spectrometry

Quadrupole mass filter operation with auxiliary quadrupolar excitation: theory and experiment

N.V. Konenkov[a], L.M. Cousins[b], V.I. Baranov[b,*], M.Yu. Sudakov[a]

[a]*Department of General Physics, Ryazan State Pedagogical University, Svoboda Street 46, Ryazan, 390000, Russia*
[b]*MDS SCIEX 71 Four Valley Dr., Concord, Ontario L4K 4V8, Canada*

Received 28 November 2000; accepted 1 February 2001

Abstract

Greatly improved peak shapes are obtained by applying auxiliary quadrupolar excitation to the first stability region of a resolving quadrupole mass filter. This phenomenon is investigated theoretically and experimentally, and is conceptualized as a splitting of the Mathieu stability diagram into multiple islands, yielding multiple operating points available for ion filtering. The modified stability diagram is calculated exactly using the solutions to Hill's equation, and yields excellent agreement with experiment. All experimental measurements are made using an inductively coupled plasma mass spectrometer. Theoretical mapping of the stability diagram is confirmed using the $^{80}Ar_2^+$ ion. Peak shape enhancements are demonstrated by measuring $m/z = 39$ in the presence of an abundance of $^{40}Ar^+$, where an operating point is found that gives $>1000\times$ increase in abundance sensitivity and also yields only a weak broadening with increasing translational ion energy up to 20 eV. Good separation of high concentrations of $^{69}Ga^+$ and $^{137}Ba^{2+}$ is demonstrated. (Int J Mass Spectrom 208 (2001) 17–27) © 2001 Elsevier Science B.V.

Keywords: Quadrupole mass filter; Resonance excitation; High order resonance; Stability "islands"; Abundance sensitivity; Resolution

1. Introduction

Since the discoveries by Paul and Steinwedel in 1953 [1] and Paul and Raether in 1955 [2] of the useful properties of rf quadrupole fields for charged particle trapping, a large amount of theoretical and experimental work [3–12] has been carried out to improve the operation of ion traps and quadrupole mass filters (QMFs). Precise electrode manufacturing, coupled with a variety of ion sources, fast electronics and ion detectors, and, for ion traps, axial ejection methods [13,14], transformed the quadrupole devices into state of the art scientific instrumentation for analytical applications.

The resonant excitation of ions by an auxiliary rf signal has proven to be a fruitful and powerful means to control the trapped ion motion. Its use markedly enhanced the ion trap performance [15], including mass selective ejection at variable q, mass range extension to low q, and the promotion of collision induced dissociation and endothermic reactions.

The theory of resonant excitation is well developed [8,15–19]. March and co-workers provided the first theoretical treatment of first order resonances resulting from auxiliary quadrupolar excitation in an rf quadrupole ion trap [8]. More recently, quadrupolar resonances were observed in a three-dimensional ion trap by Razvi et al. [20] at frequencies corresponding to integral fractions of the ion secular frequency.

* Corresponding author. E-mail: baranovi@SCIEX.com

PII S1387-3806(01)00375-X

In a recent article [19], first- and higher-order resonance conditions were derived theoretically, and the parametric nature of the excitation was depicted explicitly. Here it was shown that auxiliary quadrupolar excitation changes the stability conditions of an ion in the normal quadrupole field. These higher-order resonance lines due to quadrupolar excitation were recently investigated in detail by Collings and Douglas [21], who demonstrated the radial ejection of ions from a pressurized linear ion trap employing higher-order resonances.

For quadrupolar excitation in an rf-only field, multiple bands of instability appear on the Mathieu stability diagram due to first- and higher-order resonances [19], and therefore multiple ion ejection conditions can occur for the same ion at a single excitation frequency. Using a dc resolving field further increases the complexity, since the quadrupole field is characterized by two different values of β_x and β_y, and ion trajectories can resonate simultaneously in two different directions in response to the same excitation frequency. In this case, radial ejection occurs along the iso-β lines of a resolving QMF. As a result, as the excitation amplitude increases, the stability diagram splits into a number of stable areas, or islands, each with its own operating point and mass resolving capability.

In this work, we discuss and verify the theoretical predictions of modified stability diagrams, obtaining peak positions and shapes in selected stable islands close to the apex of the Mathieu stability diagram. For the relatively low excitation amplitude used here, we observe ion ejection and peak splitting due to different orders of perturbation. We directly compare the experimental results with the theoretical mapping of the stability diagram modified by the quadrupolar excitation. Experimentally we find that using quadrupolar excitation on a high precision resolving quadrupole yields greatly enhanced peak shapes and therefore enhanced abundance sensitivity. This potential for peak shape enhancement using auxiliary quadrupolar excitation on a QMF has been discussed empirically in several patents [22,23] without involving the prediction power of theory. Here we report a theoretical approach to the auxiliary quadrupolar excitation and its experimental verification.

Experiments are performed using an inductively coupled plasma (ICP) mass spectrometer with auxiliary quadrupolar excitation. Peak widths and positions are used to map out the modified stability diagram. Additional measurements are made for abundance sensitivity; an operating point is found that gives $>1000\times$ increase in abundance sensitivity near *m/z* 40 over a normal QMF, and also yields only a minor broadening with increasing translational (axial) ion energy up to 20 eV.

2. Theory of quadrupolar excitation

2.1. Ion motion equation

In the presence of additional rf voltage, the applied potential to the QMF rods is

$$V(t) = U + V\cos(\Omega t) + V'\cos(\omega t + \alpha) \tag{1}$$

where U is a direct voltage and V is a sinusoidal (zero to peak) voltage of the main trapping rf signal; V' is a sinusoidal (zero to peak) voltage of the auxiliary rf signal; Ω and ω are the respective angular frequencies, and α is the phase shift between them. Equations of ion motion in a quadrupole field may be expressed as follows [8,13]:

$$\frac{d^2x}{dt^2} + \frac{\Omega^2}{4}[a + 2q\cos(\Omega t) + 2q'\cos(\omega t + \alpha)]x = 0, \tag{2a}$$

$$\frac{d^2x}{dt^2} + \frac{\Omega^2}{4}[a + 2q\cos(\Omega t) + 2q'\cos(\omega t + \alpha)]y = 0, \tag{2b}$$

$$\frac{d^2z}{dt^2} = 0 \tag{2c}$$

where

$$a = \frac{8eU}{m\Omega^2 r_0^2}; \qquad q = \frac{4eV}{m\Omega^2 r_0^2}; \quad q' = \frac{4eV'}{m\Omega^2 r_0^2} \tag{3}$$

r_0 is the field radius [6] and a, q, and q' are Mathieu parameters.

The parameter q' is a dimensionless measure of the voltage V' and can be called the excitation parameter. It can be expressed as $q' = qV'/V$. In the present work, the ion motion close to the apex of the first stability island ($a_0 = 0.236\,99$ and $q_0 = 0.706\,00$) is investigated. Hence, the excitation parameter may be expressed as $q' = 70.6V'/V$ (%) and easily associated with the experimentally measured values of V and V'.

2.2. Conditions of the quadrupolar excitation resonance

In the absence of excitation, the stable ion trajectory has a quasiperiodic character. Its frequency spectrum consists of the infinite number of harmonics that are not multiple to a fundamental one [24]:

$$\omega_n = |n\Omega + \omega_s|; \quad n = 0, \pm 1, \pm 2, \ldots; \quad \omega_s = \frac{\Omega\beta}{2}. \tag{4}$$

Here ω_s is the secular frequency, and $\beta<1$ for the first stability island (region). According to Eq. (1) quadrupolar excitation has a parametric nature. In general, in the process of the parametric excitation, K excitation quanta with angular frequency ω are absorbed giving rise to two quanta of ion oscillation [25]. Hence, the most common condition of resonance using quadrupolar excitation may be expressed in terms of energy conservation:

$$K\omega = |n\Omega - \omega_s| + |m\Omega + \omega_s|; \quad m,n \text{ integers} \tag{5}$$

It is well known [26] that parametric resonance appears in a band of frequencies near resonant one. The strength of the resonance depends on ω/Ω, β, and on the excitation parameter q'. It is found by numerical simulation of the ion trajectories in previous investigation [19] that in the case of a small excitation frequency ω, the strongest resonance appears at frequencies

$$K\omega = \begin{cases} 2\omega = \Omega\beta; & \beta \approx 0 \\ \Omega - 2\omega_s = \Omega(1-\beta); & \beta \approx 1 \end{cases} \tag{6}$$

Here K=1,2,3,. . . represent the order of the resonance. In case of $\beta\rightarrow 0$, the envelope frequency equals the secular frequency, which is the lowest frequency of the ion motion [Eq. (4)]. For $\beta \approx 1$, the ion motion is more complex, and has a characteristic periodic (beat) pattern. This beat motion is created by two harmonics $\Omega\beta\backslash 2$ and $\Omega - \Omega\beta/2$ [$n = 0$ and -1 in Eq. (4)]. The frequency of the beat envelope equals $\Omega - \Omega\beta$ and it is not present in the frequency spectrum of the ion vibration [see Eq. (4)], but does define the frequencies of parametric resonance in the case $\beta \approx 1$. In both cases, the frequency on the right-hand side of Eq. (6) is twice the frequency of the ion vibration envelope, and is commonly referred to as a parametric resonance on the envelope frequencies. In this case, the ion amplitude grows exponentially at the resonance, leading to instability.

Let us consider the ion motion with parameters close to the apex of the first stability region. In this case, $\beta_x \rightarrow 1$ and $\beta_y \rightarrow 0$. With fixed small excitation frequency ω, the resonance will appear near iso-β lines:

$$\beta_Y = K\omega/\Omega; \quad \beta_X = 1 - K\omega/\Omega; \quad \omega \ll \Omega \tag{7a}$$

The instability bands appear near these iso-β lines across the Mathieu stability diagram. Similar instability bands will appear in the case when the excitation angular frequency ω is close to the main trapping angular frequency Ω:

$$\beta_X = 1 - K|1 - \omega/\Omega|; \quad \beta_Y = K|1 - \omega/\Omega|; \quad \omega \approx \Omega \tag{7b}$$

Excitation at these instability bands in x and y lead to resonance absorption; as the excitation parameter q' is increased, the absorption width broadens, and the stability diagram begins to split into islands. The method of calculating these excitation bandwidths of the stability diagram is presented in Sec. 2.3.

2.3. Calculation of the width of the instability for a range of excitation parameters

The stability of the ion oscillations with auxiliary quadrupolar excitation can be exactly calculated over

a range of excitation parameters q' in the case when the excitation angular frequency ω equals to $M/N\ \Omega$, where M and N are integers. In this instance the equations of ion transverse motion [Eqs. (2a) and (2b)] are periodic with period NT (here $T = 2\pi/\Omega$—the period of the main trapping potential), and the general theory of Hill equations [24] is applicable. The stability of the general solution of the Hill equation with NT-periodic coefficient is defined by

$$S_u = \frac{1}{2}\left(u_1 + \frac{du_2}{dt}\right)_{t=NT}; \qquad u = (x,y) \tag{8}$$

Here $u_1(t)$ and $u_2(t)$ are two particular solutions of this equation with special initial conditions:

$$u_1 = 1;\ \ du_1/dt = 0;\ \ u_2 = 0;\ \ du_2/dt = 1 \quad \text{at } t = 0 \tag{9}$$

If the general solution is stable, then $|S|<1$. If $|S|>1$ the solution is unstable due to the parametric resonance. Hence, in order to define the stability of the general solution, we have to calculate two special solutions of this equation during one full period. This is done by a numerical method. S_x and S_y are calculated for each value of a and q in order to plot the stability diagram for the given value of excitation parameter q'. If both $|S_x|$ and $|S_y|<1$, a stable point (a,q) is encountered. In the opposite case, an unstable point on the plane of (a,q) parameters is found. This method of diagram calculation will be described in detail elsewhere.

Fig. 1 presents an example of a calculated modified stability diagram, here using quadrupolar excitation at $\omega = \Omega/10$. The unstable bands are positioned along iso-β lines; this corresponds to simultaneous excitation of $n = 0$ in y and $n = -1$ in x. A set of diagrams is presented in Fig. 1(a)–(c) for $q' = 0.25\%$, 0.5%, and 1%. It is evident that the widths of the unstable bands increase with increasing excitation parameter q', and that higher-order bands (e.g. $K = 2$) also become more apparent with increasing q'. Conceptually, the stability diagram splits into several stable islands, all of which can be used in some way for ion filtering purposes. Fig. 1(c) shows the most evident islands, which are those labeled **A**, **B**, **C**, and **D**. Here islands

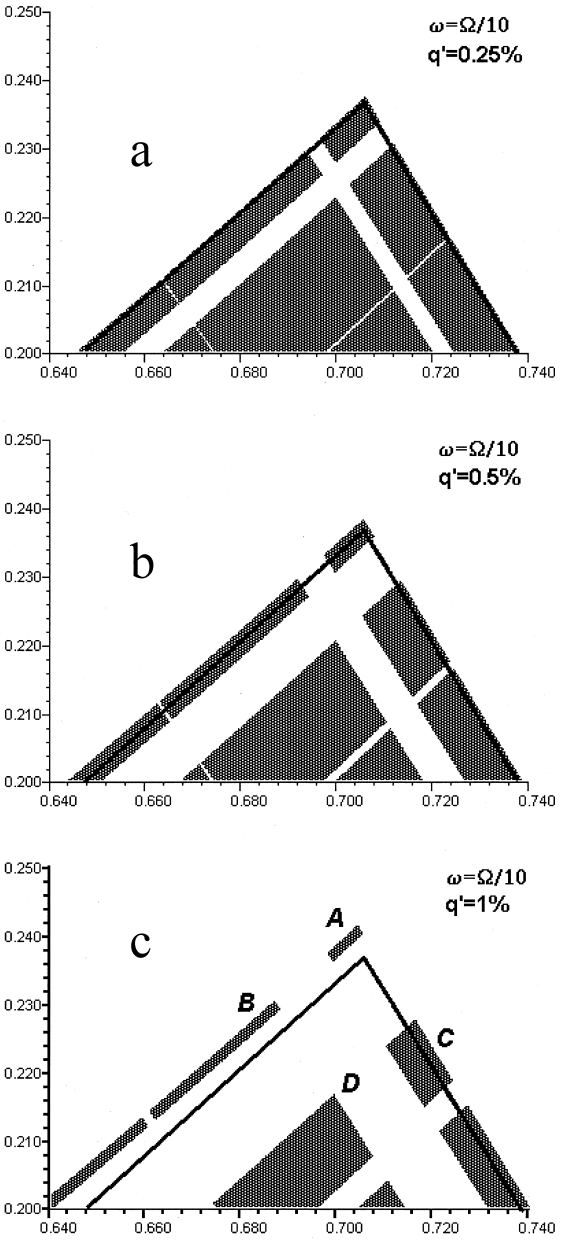

Fig. 1. Mathieu stability diagram splitting (close to apex) due to quadrupole excitation by the auxiliary signal $\omega = 0.1\ \Omega$ with excitation parameter (a) $q' = 0.25\%$; (b) $q' = 0.5\%$; (c) $q' = 1\%$.

A and **B** are narrow and **C** and **D** are wide. Interestingly, as q' increases, the stable ion boundaries move outside the boundaries of the normal Mathieu stability diagram.

For ion filtering, a scan line is used in the same manner as a normal QMF. Ions with different mass to charge ratio have a and q parameters at the (a,q) operating point positioned along a scan line $a = \lambda 2q$. Therefore, typically, the QMF operation employs a mass scan with constant ratio $\lambda = U/V$. The value of λ defines the slope at which the scan line crosses the upper tip of the Mathieu diagram, and determines the range of ions of a particular *m/z* which remain stable in the QMF. Referring to Fig. 1(c), in case of the auxiliary quadrupole excitation, the scan line with slope λ can cross island **A** only, or two islands **B** and **C**, or the three islands **B**, **C**, and **D**, depending on λ and the excitation parameter $q.'$ In these cases, single, double, or triple overlapped mass spectra can be observed respectively. Any stable island might be used for the ion separation.

This article demonstrates theoretical and experimental results for the diagram splitting at $\omega = (9/10)\Omega$ for several excitation parameters q'. Experiments are performed at $\omega = (11/10)\Omega$ as well; however, results are very similar to $\omega = (9/10)\Omega$ and will not be discussed here.

3. Experimental

Experimental measurements using quadrupolar auxiliary excitation are made on a commercial ELAN 6000 ICP-MS (Perkin-Elmer SCIEX) containing a high precision round rod array. A summary of operating conditions is presented in Table 1. An auxiliary sine wave rf signal from an arbitrary wave function generator (HP33120) is introduced into the main drive amplifier. This provides two 180° phase-shifted sine wave signals, which couple directly to the trapping rf on the x and y poles. The ratio V'/V is held constant during the mass scan. The magnitude and frequency of excitation are measured using a spectrum analyzer (Advantest R3361A). The input signal is created by an antenna, which is placed near the resonance coil. From measuring relative signal amplitudes of two spectral components with frequencies $\omega = 2\pi f$ and $\Omega = 2\pi F$, the ratio V'/V is determined at given mass number M.

Table 1.
Operating conditions

Sample introduction	Peristaltic pump (~ 1 mL min^{-1} uptake) Quartz Meinhard nebulizer (TQ-30-A2) Quartz cyclonic spray chamber
rf plasma source	Free-running (nominal 40 MHz) ICP 1150W (typical)
Plasma gas	15 L min^{-1} Ar
Auxiliary gas	1.2 L min^{-1} Ar
Nebulizer gas	0.91 L min^{-1} Ar
Dry plasma	No sample introduction, nebulizer gas only
Sampler/skimmer	1.14/0.88 mm diameter
Mass analyzer	Round rods, r_0 = 4.12 mm

The ICP-MS operates in mass range 5–250 Th. Experiments are performed at $m/z < 200$ u with step size of 20 pts/u. The main trapping frequency F is 2.5 MHz. Typical voltages V' of 1–4% of the trapping voltage V are utilized (≈20–80 V).

The ICP-generated ion flow is sampled through a multistage differentially pumped interface, which includes an actively cooled sampler-skimmer stage, an ion optics stage under a pressure of ≈1 mTorr, and a high vacuum QMF chamber. The interface produces ions with typical energy of 5 eV, and with an energy spread of 10 eV at the 10% level.

For ion stability mapping, the Ar_2^+ signal is generated from a dry plasma was used. For abundance sensitivity measurements, solutions are aspirated at flow rate of 1 mL/min.

4. Results and discussion

An observed mass spectrum of $^{80}Ar_2^+$, including residual krypton and nearby mixed isotopes of argon dimer, is shown in Fig. 2, using the $\omega\backslash\Omega$ ratio equal to 9/10 and q′ of 3.6% ($V' = 64.0$ V, $L = 2400$). Definition of the parameter L will be introduced in the following section. This spectrum is obtained when the scan line crosses the two stable islands **B** and **C**. The mass scale represents the transmitted q value corresponding to the position of the two islands on the

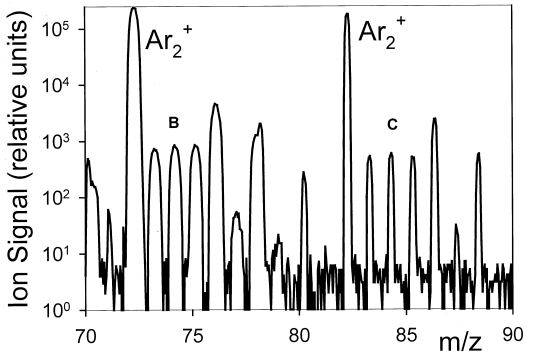

Fig. 2. Mass spectrum of $^{80}Ar_2^+$ and isotopes obtained from scanning across two excited stable islands **B** and **C**, with $q' = 3.6\%$. The ion energy is 5 eV and the quadrupole rod offset is QRO $= -2V$. Here $\omega = (9/10)\Omega$ ($\omega/2\pi = 2.25$ MHz), $V' = 64$ V, and $V = 1254$ V(p-p).

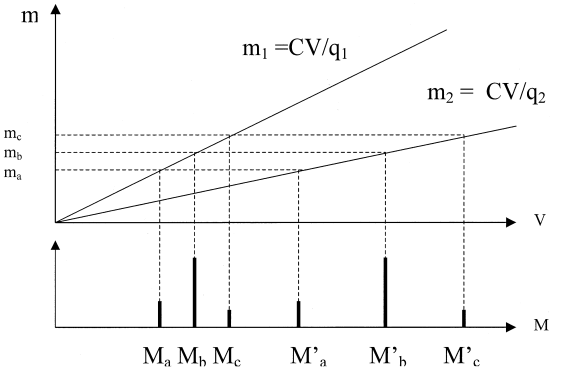

Fig. 3. Illustration of appearance of two mass spectra from two excited stable islands located along q axis at q_1 and q_2 ($q_1 < q_2$), using an ion source which produces only three types of ions with masses m_a, m_b, and m_c.

modified stability diagram. It is evident that two similar mass spectra are obtained, each with different resolution, with island **B** yielding broader peaks than island **C**. The spectra are partially overlapped because there are multiple isotopes from the ion source. If only a single population of ions were produced by the ion source, the number of peaks would be equal to the number of the stable islands which are crossed by the mass scan line.

4.1. Method of measurement of the modified stability diagram boundaries

In order to distinguish which stable island corresponds to an observed spectrum, we estimate the q at which a mass m is transmitted for a fixed V. Considering an ideal case, we assume that the positions of the two narrow stable islands on the q axis are q_1 and q_2 at given value of the scan parameter λ. According to the definition of the Mathieu parameter q [Eq. (3)], the transmitted masses m_1 and m_2 at particular voltage V can be determined as follows:

$$m_1 = \frac{CV}{q_1}; \quad m_2 = \frac{CV}{q_2}; \quad C = \frac{4e}{\Omega^2 r_0^2} = \text{const} \qquad (10)$$

The dependencies $m_1 \sim V$ and $m_2 \sim V$ are shown schematically in Fig. 3. Neighboring masses m_a, m_b, and m_c will be stable in two islands independently and the resulting mass spectra become overlapped. The condition of mass spectra overlapping from two stability regions **B** and **C** is $m_{\min} q_2 < m_{\max} q_1$ where $m_{\min}$ and $m_{\max}$ are minimal and maximal ion masses from ion source and parameters q_1 and q_2 are determined by λ and excitation level q'. If the amplitude V increases linearly with time, the first mass spectrum will arrive from the island with lower value of q. A more complex but similar picture would be observed when scan line crosses many stable islands.

Direct comparison of the experimental and theoretical modified stability diagrams was performed by measuring $\Delta m_{0.1}$ (on 10% of the peak height) of the Ar_2^+ mass peak widths for a set of the $\lambda = U/V$ values and for each stability island. These measurements were correlated back to Δa, Δq to obtain the band pass for each stability island.

A method to obtain an accurate value for the ratio U/V is developed as follows. It is difficult to measure the scan parameter $\lambda = U/V$ ($= a_{0.706}/2q_0$) directly due to the influence of the measurement circuit on operation of the mass filter. Therefore, a relative number L, which is used as a resolution control parameter in the ELAN software, is employed to change the mass peak width Δm. Without excitation by the auxiliary rf signal, the mass spectrum with a reference mass peak (Ar_2^+ in this case) was recorded. The resolution $R_{0.1} = M/\Delta m_{0.1}$ is measured as a

function of the controlled parameter L. Knowing $R_{0.1}$, the $a_{0.706}$ value (the intersection of the scan line and $q_0 = 0.7060$ [6]) is determined using:

$$a_{0.706} = 0.236\ 99 - 0.178/R_{0.1} \tag{11}$$

Applying $\lambda = a_{0.706}/2q_0$, the resulting experimental dependence of λ versus L is

$$\lambda = 0.154 + 6.00 \times 10^{-6} L \tag{12}$$

The auxiliary rf signal causes the mass peaks to appear in shifted positions on the previously calibrated mass scale. The shifted peak position is determined as follows. Assuming that the scan line intersects two stable islands, for example, the mass peak with actual mass number M_0 will arrived at rf amplitudes V_1 and V_2 in positions M_1 and M_2 on the calibrated mass scale. With respect to apparent masses M_1 and M_2 we have:

$$V_1 = C_{1q0} M_1; \qquad V_2 = C_1 q_0 M_2 (C_1 = \text{const}) \tag{13}$$

or alternatively, with respect to the actual mass M_0:

$$V_1 = C_{1q1} M_0; \qquad V_2 = C_1 q_2 M_0 \tag{14}$$

The low mass (M_1) side and high (M_2) mass side of given mass peak (here Ar_2^+) are determined as a function of the L parameter. The difference $\Delta M = M_2 - M_1$ determines the band pass width Δa and Δq along scan line relatively to the ($a_{0.706}$, q_0) point. From Eqs. (13) and (14) one can find the boundary points a_1, q_1 and a_2, q_2 of the island **A** which are intersected by given scan line $a = qa_{0.706}/q_0$:

$$a_1 = 2\lambda q_0 \frac{M_1}{M_0}; \qquad q_1 = q_0 \frac{M_1}{M_0}$$
$$a_2 = 2\lambda q_0 \frac{M_2}{M_0}; \qquad q_2 = q_0 \frac{M_2}{M_0} \tag{15}$$

Thus by changing the slope of the scan line, the boundaries of the stable islands close to the apex of the Mathieu stability diagram can be determined. The same formula, Eq. (15) is used for measuring the boundaries of stability islands **B, C** and **D**.

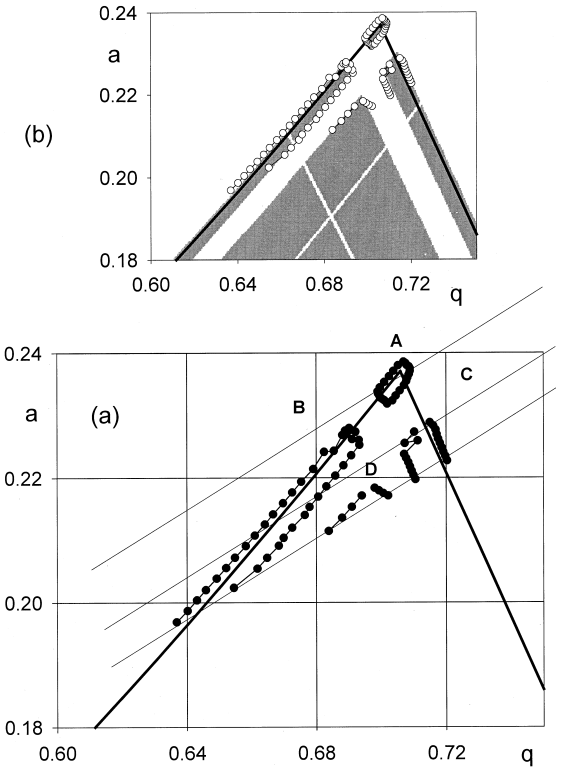

Fig. 4. Experimentally determined stable islands (a) are superimposed on the calculated diagram (b). Here $\omega = (9/10)\Omega$, $\omega/2\pi = 2.25$ MHz, and the excitation parameter $q' = 1.2\%$.

4.2. Comparison of experimental and theoretical modified stability diagrams

The experimentally obtained stability diagrams are shown on Figs. 4 and 5 at the excitation level $q' = 1.2\%$ and $q' = 2.4\%$ for an excitation angular frequency $\omega = (9/10)\Omega = 2.25(2\pi)$ MHz. Excellent agreement between the experimental and theoretically predicted stable islands is observed [Figs. 4(b) and 5(b)]. Interestingly, at 1.2% excitation, the ion signals track relatively well the unperturbed stability diagram. However, at $q' = 2.4\%$, it is evident that there is substantial perturbation of the stability diagram. Relatively small auxiliary signal, in this case, leads to dramatic change in the stability diagram.

Fig. 4 displays the experimental results of mapping the first order quadrupole resonance at $q' = 1.2\%$. This resonance is created by the excitation of the

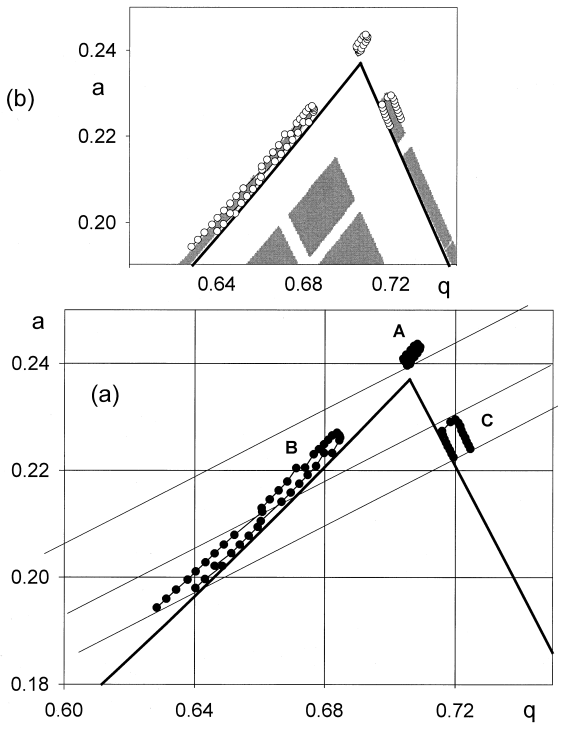

Fig. 5. Experimentally determined stable islands (a) are superimposed on the calculated diagram (b) Here $\omega = (9/10)\Omega$, $\omega/2\pi = 2.25$ MHz, and the excitation parameter $q' = 2.4\%$.

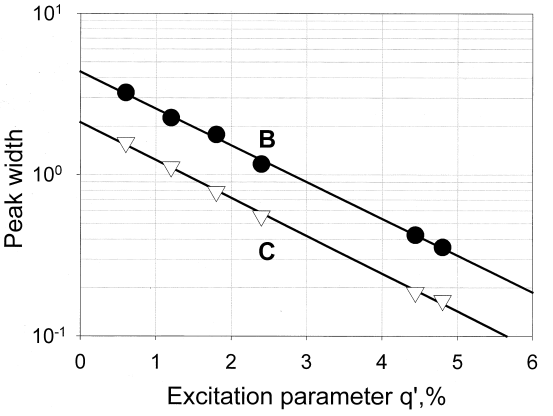

Fig. 6. Ar_2^+ peak width ($\Delta m_{0.1}$) vs. the excitation parameter q'% for the stable islands **B** and **C**.

instability bands which follow iso-β lines $\beta_x = 0.9$ and $\beta_y = 0.1$. It is evident that even with relatively low amplitude excitation, the stable islands "move away" from the unperturbed stability diagram. The unstable band which follows $\beta_x = 0.8$ ($K = 2$, the second order resonance) is only weakly excited, and manifests as a mass peak splitting for island **B**.

Stable islands **B** and **C** have boundaries which follow iso-β_y and iso-β_x lines, respectively. Hence, on these boundaries, the one-dimensional ion separation in y direction (island **B**) and x direction (island **C**) occurs. Under certain conditions, the apex of the internal island **D** can be observed. Slight deviation from the theoretical boundary might occur due to the finite ion separation time (i.e. finite number of cycles in the field), an imperfect quadrupole field, and the arbitrary decision to use the 10% peak height for the resolution measurements.

Experimentally determined stable islands at higher-level excitation $q' = 2.4\%$ are shown in Fig. 5. With increasing excitation amplitude, the instability bands are increased and the width of stable islands is narrowed. The islands **A**, **B**, and **C** move out from Mathieu stability boundaries. The distortion of the island **B** around the second order quadrupole resonance $K = 2$ is evident. Excellent agreement with the theoretical calculations of the diagram splitting is also observed in this case.

4.3. Peak width and transmission

The width of the stable islands along the scan line as a function of the amplitude of the auxiliary signal is obtained by measuring the width of the resulting ion peaks. The peak width is approximated as the width at 10% peak height. The measured peak width $\Delta m_{0.1}$ of the Ar_2^+ ion versus excitation level q' for islands **A**, **B**, and **C** is presented in Fig. 6. One can see that the resolution can be adjusted by adjusting q'. For example, unit resolution corresponds to the excitation level $q' = 1.4\%$ for the island **C**. The resolution control can be achieved by changing the V' amplitude or by changing the slope of the scan line at apexes of the **A** and **B** islands. Experimentally, the first approach is preferable because in that case the scan line crosses whole stable-island where the QMF acceptance is maximized. In Fig. 6 it is evident that the stable island width decreases with increasing excitation parameter

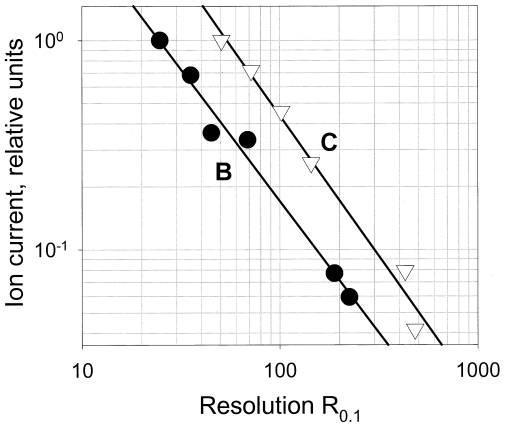

Fig. 7. Relative intensity of the Ar_2^+ signal vs. the resolution $R_{0.1}$ controlled by the amplitude of the auxiliary signal for stable islands **B** and **C**.

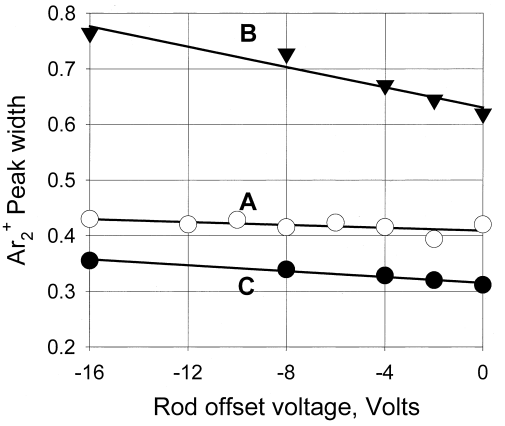

Fig. 8. Influence of the ion axial energy on the mass peak width ($\Delta m_{0.1}$) broadening for islands **A**,**B**, and **C**.

q'. For the island **B** the working range of the excitation parameter q' is between 2.8% and 4%, approximately.

The dependence of the normalized Ar_2^+ intensity on resolution $R_{0.1}$ for islands **B** and **C** are shown in Fig. 7. Again, the amplitude of the auxiliary rf signal controls the resolution. The ion transmission dependence on resolution is $I \sim (R_{0.1})^{-1.3}$, which is weaker than a normal QMF operation at apex of the Mathieu stability diagram [6].

4.4. Peak width dependence on residence time of an ion in the QMF

The peak width is nearly independent of resident time through the QMF, in contrast to normal operation at the apex of the Mathieu stability diagram. The peak width $\Delta m_{0.1}$ versus the offset voltage U_{ro} for islands **A**, **B**, and **C** and excitation levels 1.2% and 3.6% is presented in Fig. 8. Experimentally, the residence time is decreased by increasing the ion energy through the QMF, which is done by increasing the QMF offset voltage with respect to ground. The mass peak broadening with increasing the transport ion energy up to 20 eV is insignificant, especially for the two islands **A** and **C**.

In addition, increasing the ion energy up to 20 eV can increase the sensitivity up to nearly 5 times. Although the limiting resolution in comparison with conventional operation is not increased considerably, the auxiliary excitation dramatically improves the abundance sensitivity by efficient removing of the peak tails. As will be discussed below, the near independence of the mass peak width on ion residence time in the QMF directly translates into increase in the abundance sensitivity.

4.5. Abundance sensitivity

Along with relative insensitivity to ion energy, markedly enhanced abundance sensitivity has been observed. Here we define abundance sensitivity as the ratio of the largest intensity of a large peak to a neighboring small peak that still yields 10% valley separation. High abundance sensitivity is useful for applications requiring accurate quantitative measurements of two neighboring or nearby peaks of radically different concentrations. A typical commercial instrument obtains an abundance sensitivity of 10^6–10^7 [27]. The excellent abundance sensitivity is illustrated in Fig. 9 where the mass spectra without and with quadrupole excitation of island **A** are presented for an intense beam of $^{40}Ar^+$ and its neighbor $m/z = 39$. It is apparent that the mass peak tails vanish. An abundance sensitivity of approximately 10^9–10^{10} (Figs. 2 and 9) is achieved. For the ICP ion source, which has relatively large ion energy spread (up to several

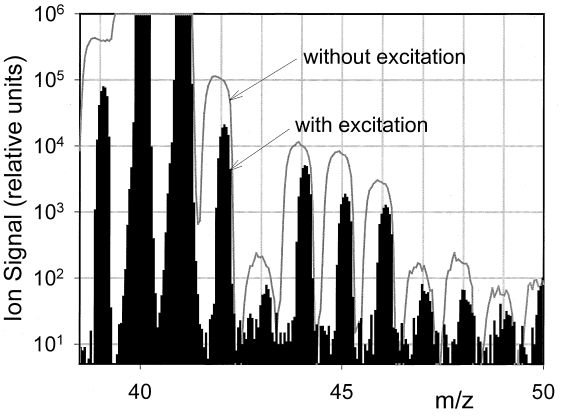

Fig. 9. Resolving of *m/z* 39, 40, and 41 using the quadrupole excitation. Upper stable island **A** (centered near *m/z* 40) was used. Foreground mass peaks are registered with excitation $\omega = (9/10)\Omega$, $\omega/2\pi = 2.25$ MHz, and $q' = 1.2\%$ ($V' = 10.7$ V). The scan parameter L is equal to 2540.

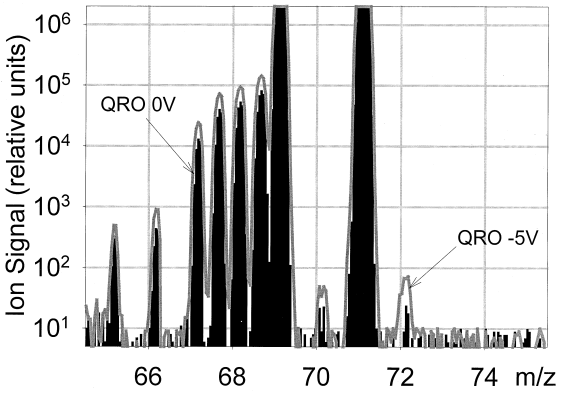

Fig. 10. Mass spectrum of 10 ppm mixture of Ga and Ba employing the quadrupole resonant excitation. Removing the peak tails on the $^{69}Ga^{+}$ ion signal allows separation of the $^{137}Ba^{++}$ signal. Two quadrupole rod offset values were used to explore dependence of the abundance sensitivity on the ion energy. Here $\omega = (9/10)\Omega$, $\omega/2\pi = 2.25$ MHz, and $q' = 1.2\%$ ($V' = 18.4$ V).

electron volts), a similar result is very difficult to achieve by other means in the first stability region.

The low mass tail in the conventional mode of the QMF operation is caused by inefficient separation at the β_y boundary [6]. The tail suppression is more efficient for islands **C** and **A**, although the **C** island requires an auxiliary mass filter for removing ions which penetrate through the island **B**. Removing the peak tails on the $^{69}Ga^{+}$ ion signal using the auxiliary rf signal allows separation of the $^{137}Ba^{++}$ signal, as illustrated in Fig. 10. Although the resolution on the 10% of the peak height is not significantly improved, the outstanding abundance sensitivity allows distinguishing between ion signals separated only by 0.5 Th and different in intensity by 10^5–10^6 times.

As stated previously, the *x* ejection of ions at the β_x boundary tends to be more efficient, thereby generating a more symmetric peak shape, than the *y* ejection of ions at the β_y boundary. In this way, one-dimensional ion separation near the $\beta_x = 1$ boundary of the island **C** is better then near the $\beta_y = 0$ boundaries of the island **B**. This can be rationalized in terms of several factors, one of which is likely the mutual orientation of the stability boundary and the scan line (Figs. 4 and 5). In the case of island **B**, the angle between the scan line $a = 2\lambda q$ and the β_y boundary is small, yielding a small change of the amplitude of the ion oscillations along the scan line. When the angle close to $\pi/2$ (as in the case island **C**, Figs. 6 and 7) the rate of change is high and the peak tails are minimized. Similarly, the rate of change $d\beta_y/dq$ is much less than $d\beta_x/dq$, yielding potentially poorer resolving power per variation of q on the β_y boundary. Finally, the nature of the ion motion at the two boundaries are very different, with the frequency at $\beta_y = 0$ rapidly decreasing and that of $\beta_x = 1$ approaching half of trapping frequency, and driving the ions at the $\beta_x = 1$ boundary may simply be more efficient. In any case, the finite residence time within the QMF amplifies these effects, leading to peak tails.

5. Conclusions

Auxiliary quadrupolar excitation is useful for creation of new stable islands on the stability diagram with new ion separating properties, and these islands can be theoretically predicted with very good accuracy. At excitation levels of 1%–3% of the trapping voltage, there is substantial increase in abundance sensitivity. Using this excitation mode of operation does not give significant increasing in limiting resolution at 10% of peak height employing the ICP ion

source; however it significantly diminishes dependence of resolution and abundance sensitivity on the ion energy.

Acknowledgements

The authors thank Graham Leith (SCIEX) for technical support and Scott Tanner (SCIEX) for fruitful discussions of the obtained data. Two of the authors (N.V.K. and M.S.) thank MDS SCIEX for financial support.

References

[1] W. Paul, H. Steinwedel, Z. Naturforschung. 8a (1953) 448.
[2] W. Paul, M. Raether, Z. Phys. 140 (1955) 162.
[3] E.W. Blauth, Dynamic Mass Spectrometers, Elsevier, Amsterdam, 1966, pp. 119–137.
[4] F.A. White, Mass Spectrometry in Science and Technology, Wiley, New York, 1968, pp. 66–107.
[5] P.H. Dawson. Adv. Electron. and Electron Phys. 53 (1980) 153.
[6] Quadrupole Mass Spectrometry and Its Applications, P.H. Dawson (Ed.), Elsevier, Amsterdam, 1976, reissued by AIP, Woodbury, New York, 1995.
[7] R.E. March, R.J. Hughes, J.F.J. Todd. Quadrupole Storage Mass Spectrometry, Wiley, New York, 1989, pp.31–110.
[8] R.L. Alfred, F.A. Londry, R.E. March, Int. J. Mass Spectrom. Ion Processes 125 (1993) 171.
[9] Y. Wang, J. Franzen, K.P. Wanczek, Int. J. Mass Spectrom. Ion Processes 124 (1993) 125.
[10] J. Franzen, Int. J. Mass Spectrom. Ion Processes 125 (1993) 165.
[11] Y. Wang, J. Franzen, Int. J. Mass Spectrom. Ion Processes, 132 (1994) 155.
[12] V.V. Titov, J. Am. Soc. Mass Spectrom. 9 (1998) 50.
[13] G.C. Stafford Jr., P.E. Kelley, J.E.P. Syka, W.E. Reynolds, J.F.J. Todd, Int. J. Mass Spectrom. Ion Processes 60 (1984) 85.
[14] G.C. Stafford, P.E. Kelley, D.R. Stephens, U.S. Patent No. 4,540,884.
[15] R.E. March, Advances in Mass Spectrometry, Vol. 14, Elsevier, Amsterdam, 1998.
[16] R.E. March, A.W. McMahon, E.T. Allinson, F.A. Londry, R.L. Alfred, J.F.J. Todd, F. Vedel, Int. J. Mass Spectrom. Ion Processes 99 (1990) 109.
[17] F. Vedel, M. Vedel, R.E. March, Int. J. Mass Spectrom. Ion Processes 99 (1990) 125.
[18] R.E. March, J. Mass Spectrom. 32 (1997) 351.
[19] M. Sudakov, N. Konenkov, D.J. Douglas, T. Glebova, J. Am. Soc. Mass Spectrom. 11 (2000) 10.
[20] M.A.N. Razvi, X.Z. Chu, R. Alheit, G. Werth, R. Blumel, Phys. Rev. A 58 (1998) R34.
[21] B.A. Collings, D.J. Douglas, J. Am. Soc. Mass Spectrom. 11 (2000) 1016.
[22] G. Devant, P. Fercocq, G. Lepetit, O. Maulat, Patent No. FR 2,620,568.
[23] K. Miseki, Patent No. US 5,227,629.
[24] N.W. McLachlan, Theory and Application of Mathieu Functions, Oxford University Press, New York, 1947.
[25] A. Yariv, J.E. Pearson, Progress in Quantum Optics, Vol.1, J.H. Sanders, K.W.H. Stevens (Eds.), Pergamon New York, 1969.
[26] L.D. Landau, E.M. Lifshitz, Mechanics, third edition, Pergamon, Oxford, 1960.
[27] K. Blaum, Ch. Geppert, P. Müller, W. Nörtershäuser, K. Wendt, B.A. Bushaw, Int. J. Mass Spectrom. 202 (2000) 81.